Controlling grip force by maintaining a constant frictional safety margin to improve robotic grasping

by

C.A. Langens

to obtain the degree of Master of Science
at the Delft University of Technology,
to be defended on Tuesday November 29 2022.

Student number:	4440609	
Degree:	MSc Robotics	
Thesis committee:	Dr. M. Wiertlewski,	TU Delft, supervisor, chair
	Dr. L. Willemet,	TU Delft, daily supervisor
	Dr. M. Plooij,	DEMCON, daily supervisor
	Dr. J. Kober,	TU Delft, external committee member
	Dr. E. van der Kruk,	TU Delft, external committee member

TU Delft

Controlling grip force by maintaining a constant frictional safety margin to improve robotic grasping

Coco Langens

Abstract—Manipulating soft and fragile objects is a challenging task in robotic grasping. The key challenge for robotic grasping is to exert enough grip force to prevent slipping while being gentle enough to prevent damage to an object. Existing grippers used for processes like automatic harvesting of fruits, either apply excessive grip force leading to object damage or react to slip resulting in object release from the gripper. The aim of this study is to develop a grip force controller that uses tactile feedback to maintain a constant frictional safety margin over the minimum required grip force, called Safety Margin Control. Tactile sensors can provide information on friction, which is used to predict slip. An optical tactile sensor is modeled and used in simulations where Safety Margin Control regulates the grip force during interaction with various virtual objects. The deformation of the sensor's soft viscoelastic membrane is described by local frictional behavior and used to estimate the safety margin. The desired safety margin is set to 30%, based on comparison to the way humans control grip force in their fingertips. The desired value can be tuned to favor release over damage and vice versa. Safety Margin Control is compared to two baseline controllers: React To Slip and Conservative Control. The performance is evaluated based on maximum pressure and total lateral displacement of the object relative to the sensor. Safety Margin Control results in a pressure decrease of 44% on average compared to Conservative Control, and no significant pressure change was observed compared to React To Slip. The total lateral displacement for Safety Margin Control is 0 mm, as opposed to 1.3 mm for React To Slip. Safety Margin Control provides a way forward for automated harvesting as the pressure exerted on an object can be reduced while no slip occurs.

Index Terms—automated harvesting, control, friction, robotic grasping, safety margin, simulation, tactile sensing

1 Introduction

The agricultural industry copes with a global labor shortage. Between 2010 and 2019, the available work force decreased by 16% [1]. In Europe, the figure plummeted by 47% over the same time period. Due to labor shortages, farmers leave their crops unpicked or rotting in the field [2], [3]. To reduce food waste, emphasis is shifting from reliance on manual labor towards technology [4]. Humans are perfectly able to pick fruits, but robots that can grip fragile agricultural products of varying shape and size, are not available yet [5]. The aim of this study is to improve robotic grasping by developing a new controller that uses tactile feedback to control the grip force of a robotic gripper. Tactile features (e.g. texture, shape, or friction) are related to the sense of touch and obtained via physical interaction with the environment. The newly developed controller draws inspiration from the human sense of touch, where tactile features are encoded via skin deformation. The perception of these features is crucial to manipulate objects and humans fail to hold objects in a stable grasp when they are deprived from sensing skin information [6]. Above all, it was shown that frictional features dictate human grip force control [7]. Humans unconsciously regulate the grip force required to hold an object at a frictional safety margin of 10-40% to avoid slippage [8]. This principle ensures a stable, yet gentle enough grasp to prevent damage to the object. Therefore it was chosen as the basis of a new controller, called Safety Margin Control. To the best of the author's knowledge, a feedback controller that maintains a constant frictional safety margin was not developed before.

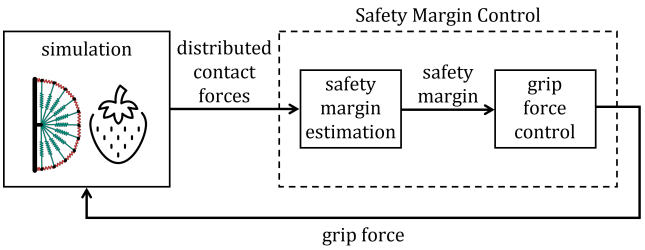

Fig. 1. The interaction between a tactile sensor and object is simulated during robotic grasping. The contact forces are used in Safety Margin Control to estimate the safety margin. The grip force is then regulated to maintain a constant safety margin of 30%.

A model of a tactile sensor is created and the controller is tested in simulation. Safety Margin Control estimates the safety margin and regulates the grip force to maintain a constant safety margin to hold various virtual objects subjected to external perturbations in a stable, yet gentle grasp (Fig. 1). The objects' properties are based on the characteristics of a strawberry as an example of a fragile agricultural product. The two metrics used to validate the performance of the controller reflect the main causes of fruit damage during grasping: compression and impact forces [9].

These forces occur when excessive grip force is applied, or when the fruit is dropped on the ground. The corresponding metrics are maximum pressure and total lateral displacement of the object relative to the sensor. The performance of Safety Margin Control is compared to two baseline controllers: React To Slip and Conservative Control. The following research question is answered: *Does a controller that maintains a constant frictional safety margin improve robotic grasping in terms of object release and damage?*

Outlook

This paper is structured as follows. Chapter 2 provides background information on human grasping, tactile sensors, and grip force control. A tactile sensor is modeled in chapter 3. Safety Margin Control and the two baseline controllers (React To Slip and Conservative Control) are presented in chapter 4. The experiments are explained in chapter 5. Chapter 6 provides the results of the experiments. Discussion and conclusions can be found in chapter 7 and 8.

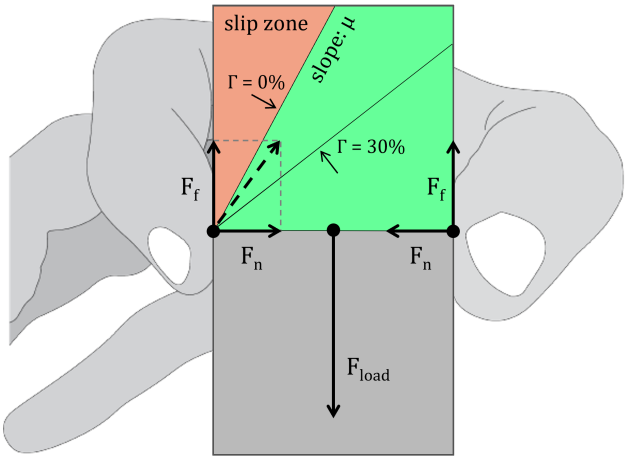

Fig. 2. Contact forces while holding an object. The grip force F_n is applied perpendicularly to the contact surface between object and finger. The friction force F_f develops tangentially to the contact surface and opposes motion in the direction of the load F_{load}. The grasp is stable when the resulting force (dashed arrow) points in the green area ($\Gamma > 0\%$). However, the resulting force depends on the grip force and slip occurs when it points in the orange area ($\Gamma \leq 0\%$). Adapted with permission from [11]

2 Background

Human grasping

When humans manipulate objects, tactile information on shape, texture and friction is used to adjust the grip force and prevent excessive forces or slip. These properties are acquired via physical interaction with the environment. First, action potentials are generated by tactile receptors in the skin when they are stimulated by e.g. mechanical deformation, pain or heat [10]. The central nervous system then uses these signals to adjust the applied grip force during object manipulation. Research has shown that frictional properties are of major importance for grip force control [7]. Friction and slip are closely related and humans can predict when slip will occur from the contact forces that arise in our fingertips during manipulation (Fig. 2). It was shown that humans always apply a constant frictional safety margin of 10-40% over the minimum required grip force to prevent slip [8]. The grip force (F_n), friction force (F_f), and safety margin (Γ) can be related using Coulomb's law (1).

$$(1 - \Gamma) \cdot F_f \leq \mu F_n, \tag{1}$$

where μ represents the object's friction coefficient. Coulomb's law states that slip occurs when the load force exceeds the maximum friction force. Following this, the maximum friction force is defined by μF_n. Thus, the safety margin can be calculated if the grip force, actual friction force and friction coefficient are known (1). No machine can emulate the outstanding human ability to effectively manipulate a wide range of objects independently of how fragile, heavy or slippery they are. Therefore, it is chosen to exploit the safety margin in a robotic grip force controller.

Tactile sensors

Tactile sensors provide information on characteristics such as texture, shape or friction. State-of-the-art tactile sensors are often vision-based as a result of the availability of affordable high-resolution cameras and the development in computer vision techniques. Some of these sensors can measure both normal contact force and friction force during manipulation [12], [13]. As these properties are needed to calculate the safety margin, an optical tactile sensor is used to create a sensor model. In particular, one sensor is used, called ChromaTouch [12]. The sensor can be integrated in a robotic gripper (Fig. 3a) and tactile perception originates from the mechanical deformation of a soft hemispherical fingertip (Fig. 3b). The sensor consists of two transparent silicone layers which both contain colored markers. The sensor deforms under contact and a camera tracks the markers' displacement and color change. The optical image can directly be linked to the displacement of the markers with respect to the camera frame. The output is a distributed deformation field at contact. Using a model avoids the need for labor-intensive real-life tests and data augmentation.

Friction coefficient estimation

An object's friction coefficient is required to calculate the safety margin. It is commonly assumed known in current research on robotic grasping [16]. In reality, the friction coefficient is neither known in advance nor constant due to e.g. weather conditions, moist or sand. Therefore, it has to be estimated to apply Safety Margin Control in realistic applications. It is shown that an object's friction coefficient can be estimated on initial contact with the ChromaTouch sensor [17].

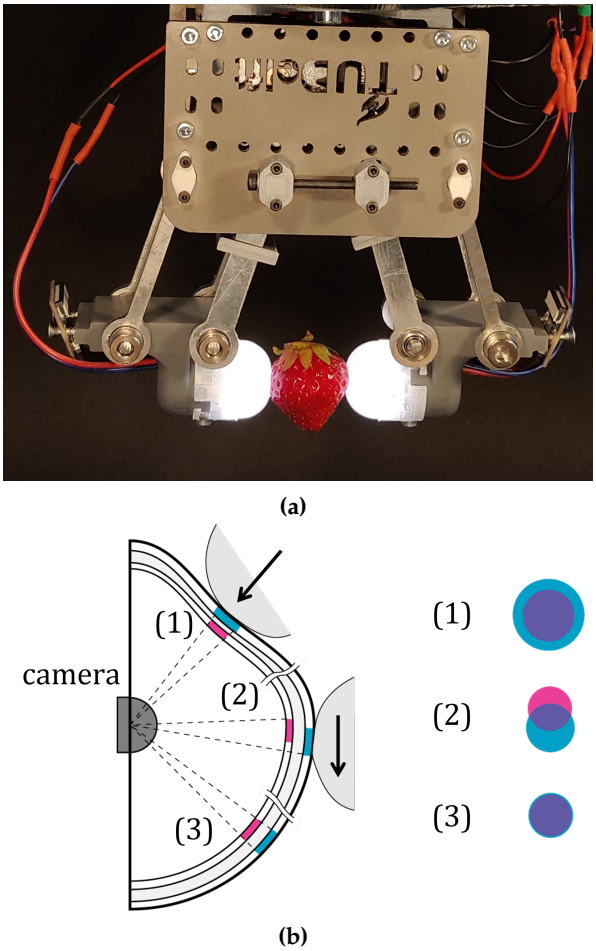

Fig. 3. (a) Tactile sensors (white hemispheres) integrated in a robotic gripper [14]. (b) The soft hemispherical sensor consists of two transparent silicone layers with colored markers. The sensor deforms under compression (1) and shear (2). The optical image can be linked to displacement with respect to the camera. Adapted with permission from [15].

Control methods

Two existing methods to control robotic grippers are React To Slip and Conservative Control.

React To Slip. The most advanced controller that includes tactile features in grip force control is React To Slip, the first baseline controller used in this study. In order to exploit this method, information is needed on when slip occurs. This measure of slip is provided by optical tactile sensors as relative displacement between an object and a tactile sensor. The lateral displacement has to exceed a threshold of 1-15 mm before displacement is classified as slip [18], [19]. When the threshold is exceeded and slip occurs, React To Slip control increases the grip force with a predefined amount of force up to 10 N [20], [21], or with a predefined percentage of 10% [22]. A disadvantage of React To Slip is that it does not prevent slip, whereas slip should be prevented since it can lead to release of the object from the gripper.

Conservative Control. The second baseline controller is Conservative Control. This method is commonly used to control industrial robots that execute simple and repetitive tasks. These robots are deployed in controlled factory environments and only have to handle objects with similar weight, stiffness, and texture. The applied grip force is an overestimation of the required force. Using Conservative Control, robots cannot handle the variety we see in fruit and, e.g. ripe fruit will be squeezed. Robotic grippers available on the market cannot be controlled at less than 5 N, while strawberries already get damaged at 3.5 N [23]. Despite the fact that Conservative Control is not appropriate for handling delicate objects like strawberries, it is currently the most widely used method to control robotic grasping, hence it is utilized as a baseline.

3 TACTILE SENSOR MODEL

A model of a tactile sensor is created to test the performance of Safety Margin Control in simulation. The tactile sensor is modeled using the numerical two-dimensional model of a fingertip from [24], called Fingertip Model. The Fingertip Model takes both friction and viscoelasticity into account, which are difficult to model [25], [26]. At the same time, it only needs 4 parameters (2 spring stiffnesses, damping coefficient and finger radius) to predict mechanical deformation and contact forces during interaction with objects of varying properties (curvature, stiffness and friction coefficient).

The Fingertip Model consists of a chain of massless nodes connected by springs (Fig. 4). The external springs (red) represent the elastic silicone. The internal springs (green) maintain the shape of the sensor, and the dampers model the viscosity of the sensor dome. The parameters required to define the model are 2 spring stiffnesses (k), a damping coefficient (c), the sensor radius (r), Poisson factor (ν), and the number of nodes (N_n) (Table 1). An overview of all symbols used in this chapter can be found in Appendix A.

TABLE 1. Parameters used to define the Fingertip Model.

Parameter	Definition	Value
k	spring stiffness	k_{int} = 314 N/m, k_{ext} = 1544 N/m
r	radius sensor	8 mm
c	damping coefficient	0.1 Ns/m
ν	Poisson factor	ν_{int} = 0.4 , ν_{ext} = 0.004
N_n	number of nodes	251

Dynamics. The motion of the nodes is modeled using the equations of motion for a mass-spring-damper system (2). Inertia is ignored since the nodes are massless.

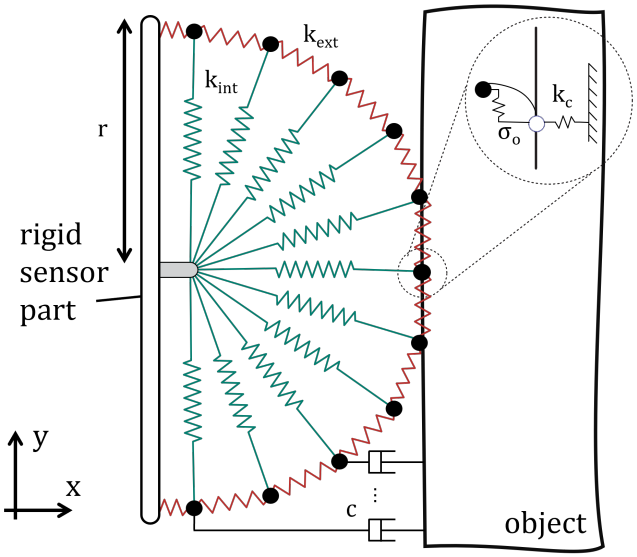

Fig. 4. Tactile sensor model where nodes (black) are connected via springs and dampers. Parameters k_{int} and k_{ext} represent the stiffnesses of the internal (green) and external (red) springs, respectively. c is the damping coefficient and r the sensor radius. The parameters k_c and σ_0 define the contact between the object and the sensor and are therefore not included in Table 1.

$$c \begin{bmatrix} \vec{\dot{x}} \\ \vec{\dot{y}} \end{bmatrix} + \vec{k} \begin{bmatrix} \vec{\Delta x} \\ \vec{\Delta y} \end{bmatrix} + \begin{bmatrix} \vec{F}_x \\ \vec{F}_y \end{bmatrix}_{ext} = 0 \tag{2}$$

Spring forces. Every spring connects two nodes and is split in a horizontal and vertical component (Fig. 5). The x- and y-component of the spring force (F_{spring}) are calculated based on the displacement Δx and Δy caused by external force F (3). The factor ν accounts for the Poisson effect that describes a material's tendency to expand perpendicular to the direction of compression, i.e. it causes a displacement in horizontal direction, when only a vertical force is applied.

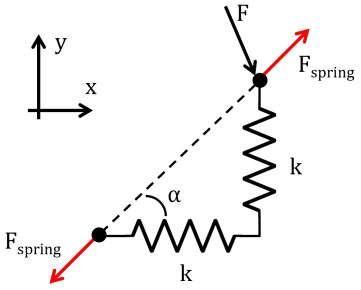

Fig. 5. Definition of spring force in the Fingertip Model. The spring (dashed line) between two nodes (black dots) is split in a horizontal and vertical component. Force F causes a displacement that induces the spring force (red).

$$\begin{aligned} F_{spring,x} &= \cos(\alpha) \cdot k \cdot \Delta x - \sin(\alpha) \cdot k \cdot \nu \cdot \Delta y \\ F_{spring,y} &= \sin(\alpha) \cdot k \cdot \Delta y + \cos(\alpha) \cdot k \cdot \nu \cdot \Delta x \end{aligned} \tag{3}$$

Equation 3 provides the force resulting from a single spring, but the Fingertip Model consists of multiple springs. Extending equation 3 to cover the entire model requires the multiplication of a large stiffness matrix (Fig. 6). Every matrix entry represents a trigonometric function that depends on the orientation of the springs, so the matrix has to be repopulated at each time step. N_n + 1 includes all nodes and the rigid sensor part.

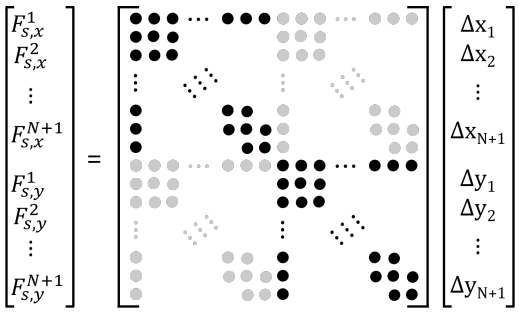

Fig. 6. Structure of stiffness matrix $\vec{k}$ for all springs. The size of the matrix is 2(N_n+1) x 2(N_n+1). There are N_n nodes and the spring force acting on each node is calculated. Every dot in the matrix represents a trigonometric function that describes the orientation of the corresponding spring. The Poisson effect is reflected by the gray parts. $F^1_{s,x}$ and $F^1_{s,y}$ describe the spring force acting on the rigid sensor part that is connected to multiple springs, therefore these rows differ from the other rows.

Contact interaction. The contact forces can be resolved in two components: contact force acting perpendicular to the contact surface (F_n) and friction force acting tangentially to the contact surface (F_f).

Normal contact force. The normal contact force is calculated by modeling the object's surface as a spring with a high stiffness k_c (Fig. 7a). Each node in contact with the object is counteracted by a high stiffness spring (4). Stiffness k_c can be changed to simulate stiff or compliant objects.

$$F_n = k_c \cdot x \tag{4}$$

Friction force. The local friction force F_f is modeled according to the Dahl friction model as shown in Fig. 7b [27]. Equation 5 gives the mathematical representation

$$\begin{aligned} \dot{F}_f = \sigma_0 \cdot \left| 1 - \frac{F_f}{\mu \cdot F_n} \operatorname{sign}(\dot{y}) \right|^n \\ \cdot \operatorname{sign}\left(1 - \frac{F_f}{\mu \cdot F_n} \operatorname{sign}(\dot{y}) \right) \cdot \dot{y}, \end{aligned} \tag{5}$$

where σ_0 is the stiffness of the bristle, μ the friction coefficient and n a material dependent parameter. n is ≥ 1 for ductile materials and < 1 for brittle materials.

4 Controllers

Safety Margin Control and the two baseline controllers (React To Slip and Conservative Control) are presented in this chapter.

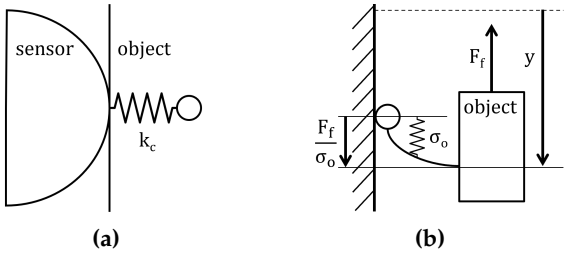

Fig. 7. Contact interaction. (a) Normal contact force with high stiffness springs k_c. (b) Friction force according to Dahl model.

4.1 Safety Margin Control

Safety Margin Control is a newly developed feedback controller that regulates the grip force (F_{grip}) to maintain a constant desired safety margin (Γ_{des}) over the minimum required grip force (Fig. 8). The grip force is controlled with a PI-controller (6). The grip force is governed by the error (e) of the current and the desired safety margin. The term $u_{forward}$ is a feedforward term that decreases the error by predicting the required force needed to grasp a strawberry. It is set to 0.5 N which is an approximation of the force needed to lift an average strawberry. The gains K_p and K_I are tuned manually and set to 2.5 and 0.1, respectively.

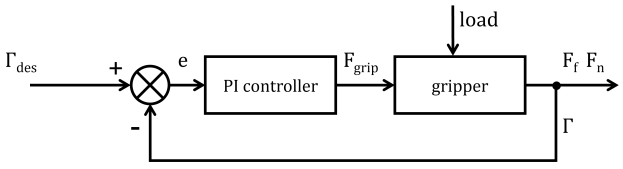

Fig. 8. Safety margin (Γ) control diagram.

$$F_{grip} = u_{forward} - K_p e - K_I \int e\, dt$$
$$e = \Gamma_{desired} - \Gamma \tag{6}$$

The safety margin can be calculated from the normal contact force (F_n), friction force (F_f), and the object's friction coefficient (7).

$$\Gamma = \frac{\mu_{est} \cdot \sum F_{n,i} - \sum F_{f,i}}{\mu_{est} \cdot \sum F_{n,i}} \tag{7}$$

F_n and F_f are outputs of the tactile sensor. They are presented as a distributed force field and $F_{n,i}$ and $F_{f,i}$ represent the contact forces for one marker. The sum of the forces of all markers in contact with the object is used to calculate the safety margin. The object's friction coefficient μ_{est} cannot directly be obtained from the sensor's output and has to be estimated.

Friction coefficient estimation. An estimation of the object's friction coefficient is required to calculate the safety margin (7). The local friction coefficient can be obtained from the contact forces using Coulomb's friction law ($F_{f,i} = \mu F_{n,i}$), since the law is locally valid for elastic surfaces in contact [28]. The local friction coefficient differs per node and also varies for different values of the safety margin (Fig. 9). The estimated friction coefficient μ_{est} is calculated by taking the maximum value of all local friction coefficients (8). A moving average with a window of 50 time intervals is applied to filter out large deviations.

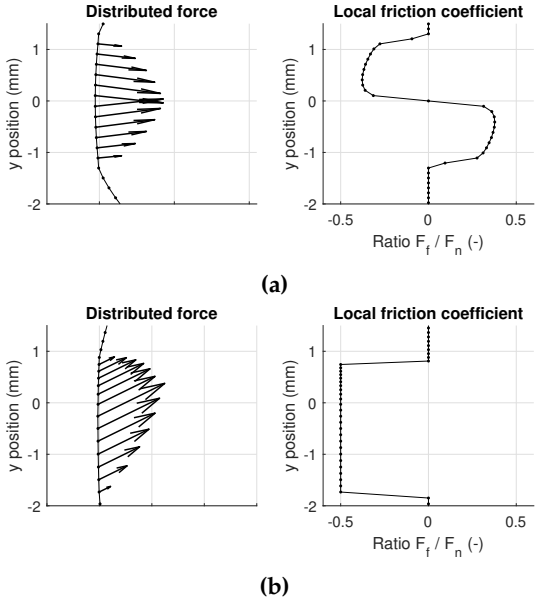

Fig. 9. Distributed contact forces and corresponding local friction coefficients. The object has a real friction coefficient of 0.5. (a) Sensor is pushed against an object and no slip occurs (Γ = 100%). (b) Object slips (Γ = 0%).

$$\mu_{est} = \max_{i \in N} \left\{ \frac{|F_{f,i}|}{|F_{n,i}|} \right\} \tag{8}$$

The approach to estimate the friction coefficient is validated by means of the following experiment. The sensor is pressed against 3 objects, each with a different friction coefficient (μ = {0.3, 0.5, 0.7}). A grip force of 1 N is applied to the sensor until a steady state is reached (Fig. 10). Then, a load of 0.1 N is applied to the object. The results show that, before the load is applied, the estimated friction coefficient only approaches the real friction coefficient (μ_{real}) when μ_{real} = 0.3 (yellow line). The estimates for a real friction coefficient of 0.5 and 0.7 both equal 0.4 on initial contact. After addition of the load, all three estimates approach μ_{real}. To explain this observation it should be noted that the local friction coefficient (μ_{est}) only approaches μ_{real} when local slip occurs. The threshold to slip increases for an increasing real friction coefficient. Local slip only occurs on initial contact when μ_{real} = 0.3 (Fig. 11a). The additional load is needed to cause local slip for a friction coefficient of 0.7 (Fig. 11b). In this study, a load will always be present when Safety Margin Control is switched

on. Therefore μ_{est} always approaches μ_{real} and no problems related to the friction coefficient estimation were encountered.

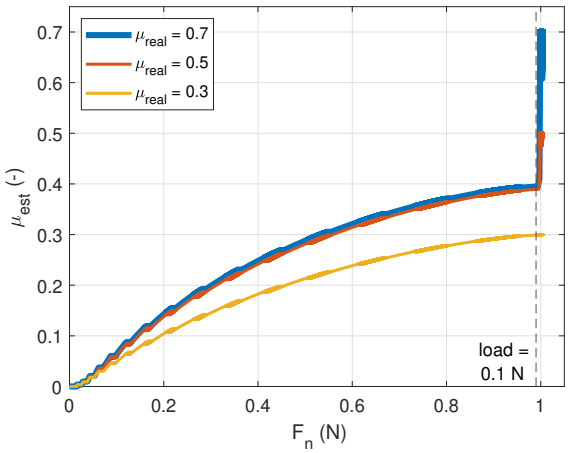

Fig. 10. Estimated friction coefficient μ_{est} plotted against the total normal force F_n. First, only grip force of 1 N is applied until a steady state is reached. Then a load force of 0.1 N is added.

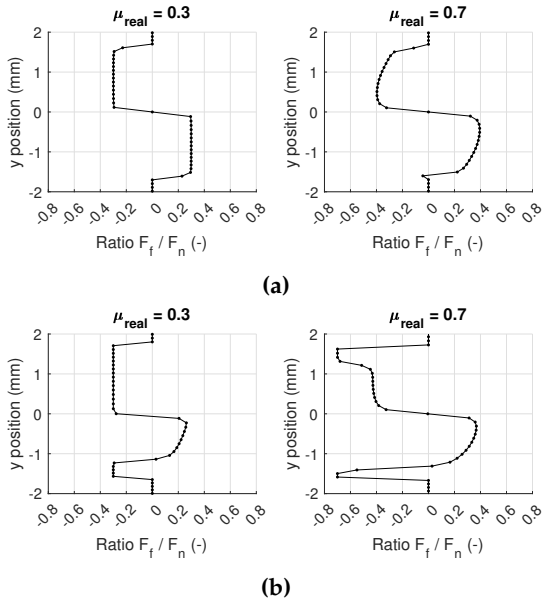

Fig. 11. Local friction coefficient for real friction coefficient (μ_{real}) of 0.3 and 0.7. The results are presented for a steady state. (a) Only grip force of 1 N is applied. (b) Both grip force (1 N) and load force (0.1 N) are applied.

4.2 React To Slip

A typical method to regain stability of a slipping object is to increase the grip force with a predefined amount of force [29], [23], [18]. The approach from James et al. is used as example [18]. In that article, the relative lateral displacement (Δy) between a tactile sensor and the object must be greater than a threshold (τ) in order to detect slip. Force F_{step} is added to the grip force when slip is detected (9). F_{step} is varied and ranges from 0.25 to 3 N. Threshold τ is set to 1.3 mm because that is the lowest observed displacement of a node in [18].

$$F_{grip} = \begin{cases} F_{grip} + F_{step}, & \text{if } \sum_{i=1}^{N} \Delta y > \tau, \\ F_{grip}, & \text{else .} \end{cases} \tag{9}$$

4.3 Conservative Control

Conservative Control exploits a constant grip force which is an overestimation of the required grip force to hold an object. The grip force is fixed at 5 N in this study (10), as this is the lowest force at which readily available tactile grippers can be controlled.

$$F_{grip} = 5 \text{ N} \tag{10}$$

5 Experiment

In the experiment a single simulated tactile sensor is pushed against an object for computational efficiency.

5.1 Controller validation

An experiment consists of three sequential phases (Fig. 12) and takes 2 seconds. The first phase is the initialization and takes 0.04 seconds. During this phase contact between the sensor and an object is established. Then, the controller is switched on and an external load is applied to the object. The load is increased halfway the experiment (t = 1 second). The increase marks the start of the final phase.

The three controllers are validated during the first experiment. Both the grip force regulation and the development of the safety margin in response to the applied load is studied. A single object is taken into consideration.

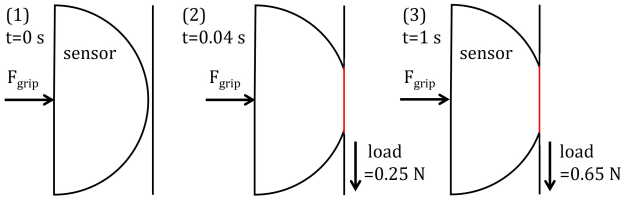

Fig. 12. Schematic view of an experiment. (1) Grip force is applied to establish contact. (2) Controller starts and load is applied. (3) Load is increased. The interaction at contact (red) is studied during an experiment.

5.2 Object properties

The controllers' effect on object damage and release is investigated based on maximum pressure and total lateral displacement of the object relative to the sensor (11). A node is considered to be in contact with the object when $F_{n,i} > 0.005$ N. The contact area is calculated as the absolute distance between the two

outer nodes in contact with the object. The development of the metrics are first shown over time for an experiment that takes a single object into account.

$$\begin{aligned} \text{pressure} &= \frac{\sum F_{n,i}}{\text{contact area}} \\ \text{lateral displacement} &= \underset{i \in N}{min}\{\Delta y_i\} \end{aligned} \tag{11}$$

The experiment is then repeated 27 times for each controller. Each repetition considers a different object. The objects vary in curvature (ρ), stiffness (k_c) and friction coefficient (μ) and are modeled according to the characteristics of a strawberry. The friction coefficient varies between 0.3, 0.5, and 0.7 [30]. The curvature ranges from 0 to 20 mm [31] and the stiffness is 200, 32 or 16 kPa [32]. The stiffness of the simulated sensor is 25 kPa. Three object properties with each three possible values gives a total of 27 objects.

5.3 Control parameters

The control parameters also affect object release and damage and were varied as well. The desired safety margin Γ_{des} and the step size F_{step} are taken into account as control parameters. Γ_{des} applies to Safety Margin Control and is adjusted from 9% to 80%. F_{step} applies to React To Slip and the studied step size spans from 0.5 N to 3 N. Conservative Control has no control parameter that can be varied. The control parameters are varied during an experiment with an object with the following properties: μ = 0.5, ρ = 0 mm, and k_c = 200 kPa.

6 Results

The experiments are divided in three parts. The behavior of Safety Margin Control and the two baseline controllers is validated first. The effect of each controller on object release and damage is then shown for 27 different objects. Finally, the effect of adjustments to the control parameters is demonstrated.

6.1 Controller validation

During controller validation, a single object with the following properties is considered: μ = 0.5, k_c = 200 kPa and ρ = 0 mm. The load and grip force are shown in Fig. 13. Safety Margin Control first decreases the grip force to 0.1 N, which is the lowest permitted grip force (blue line). Next, at first oscillations are observed and then it rises gradually. Both Conservative Control (red line) and React To Slip (yellow line) maintain a constant grip force of 5 and 0.5 N, respectively. An increase in the load marks the start of the third phase (1 - 2 seconds). Safety Margin Control again gradually increases the grip force, but no oscillations are observed this time. Conservative Control maintains a constant grip force at 5 N. Lastly,

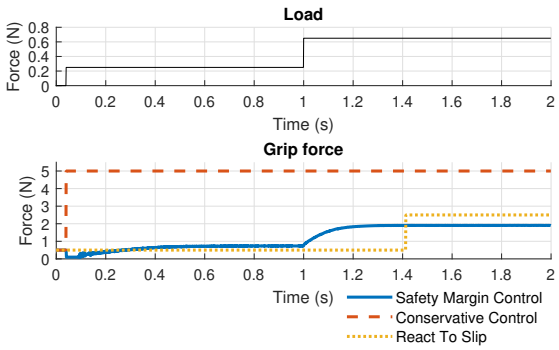

Fig. 13. Load and grip force during controller validation. The object's properties are: μ = 0.5, k_c = 200 kPa and ρ = 0 mm.

React To Slip increases the grip force with 2 N at t = 1.4 seconds.
Contact forces occur as a result of the aforementioned grip and load force and are used to calculate the safety margin (Fig. 14). The safety margin is only required for Safety Margin Control, but is also shown for the two baseline controllers to allow for comparison.

The normal contact force is shown in the top graph of Fig. 14. It is closely related to the applied grip force. The only difference is a delay in the system caused by the damping.

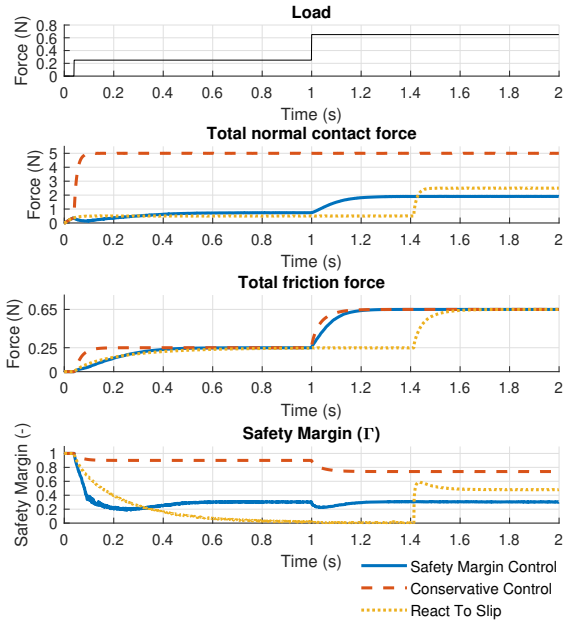

Fig. 14. Normal contact force, friction force and safety margin during controller validation. The object's properties are: μ = 0.5, k_c = 200 kPa and ρ = 0 mm.

Similarly, the friction force resembles the course of the load force (middle graph Fig. 14). The plateaus occur at the same magnitude (0.25 and 0.65 N), albeit the damping introduces a settling time before reaching

a steady-state. The settling time differs per control method and is 0.1 seconds for Conservative Control, 0.5 seconds for Safety Margin Control, and 0.7 seconds for React To Slip. When the load is increased both Safety Margin Control and Conservative Control show a direct response in friction force. Unlike React To Slip, where the friction force only starts to rise at t = 1.4 seconds.

The safety margin is 1 during initialization, which is expected since no load is applied (bottom graph Fig. 14). Safety Margin Control maintains a safety margin around 30%, which is the predefined desired value (blue line). Fluctuations in the safety margin are observed between 0.1 and 0.2 seconds similar to the observed fluctuations in the grip force. Furthermore, the controller has an overshoot of 10%. Conservative Control shows a step-wise decrease of the safety margin related to the step-wise increase in friction force (red line). Only the friction force influences the safety margin while exploiting Conservative Control, as the grip force is constant. Lastly, React To Slip shows a safety margin of 0% from 0.8 - 1.4 seconds (yellow line). Because a 0% safety margin corresponds to slip, this period marks the time it takes to meet the threshold put on slip detection for this specific experiment.

6.2 Object properties

The development of pressure and lateral displacement is first shown by means of an experiment with an object with the following properties: μ = 0.5, k_c = 200 kPa and ρ = 0 mm (Fig. 15). Pressure depends on the applied grip force and the contact area. The pressure follows the trajectory of the applied grip force for all three control methods. The curves are not completely smooth and bumps are observed during steep increases in the grip force. These bumps are caused by the discrete calculation of the contact area, because the area in- or decreases incrementally when a node establishes or loses contact. Conservative Control results in the highest pressure during the entire experiment. Safety Margin Control and React To Slip result in a lower pressure and follow a similar trend. The highest pressure is observed for React To Slip comparing only these two methods. Lateral displacement of the object relative to the sensor is only observed for React To Slip, since slip has to occur to be able to react to it. The displacement is 1.3 mm which equals the threshold put on slip detection. The displacement increases at a constant rate, since the system is massless and no acceleration takes place.

The results for the 27 different objects are presented here. The total lateral displacement and maximum pressure are compared to demonstrate the influence of each controller on object release and damage. Only

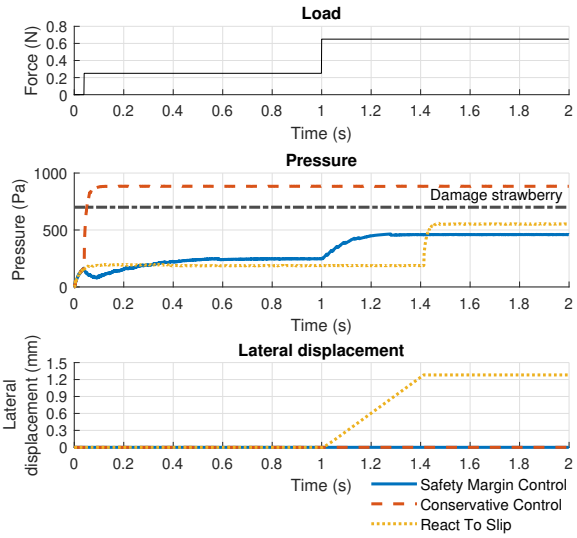

Fig. 15. Pressure and lateral displacement over time. The object's properties are μ = 0.5, k_c = 200 kPa, and ρ = 0 mm.

React To Slip results in displacement. The total lateral displacement has a constant value of 1.3 mm which is not influenced by varying the objects' properties and equals the threshold put on slip detection.

By contrast, the maximum pressure is influenced by the objects' properties (Fig. 16). There are two overarching observations. To begin with, the maximum pressure increases for a decreasing curvature, since the contact area is smaller for objects with a smaller curvature. Second, it is shown that stiffer objects result in higher maximum pressure. Only Safety Margin Control is influenced by changes in the friction coefficient and shows an increase in maximum pressure for a decreasing friction coefficient.

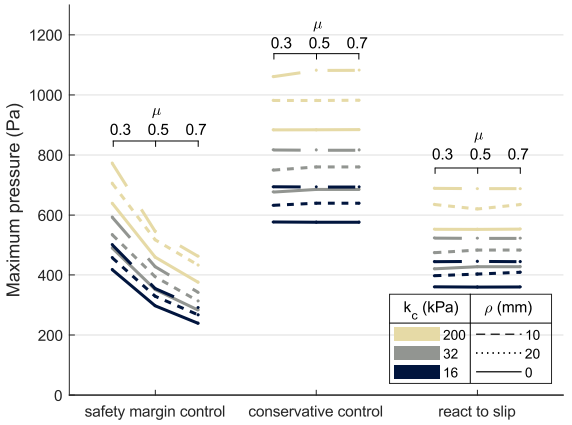

Fig. 16. Maximum pressure per object with different parameters for friction coefficient (μ), stiffness (k_c) and curvature (ρ) per control method.

In reality, an object's exact properties are not known in advance. To illustrate the effect of each controller on an unknown object the maximum pressure is aggregated for all objects (Table 2). The findings are compared to Safety Margin Control and a two-sampled t-test yielded p-values of 0.057 and $7.7\mathrm{e}^{-12}$, respectively for React To Slip and Conservative Control. As a result, at a significance level of 5%, there is only a statistically significant difference in maximum pressure between Conservative Control and Safety Margin Control. The controllers apply a different grip force, suggesting that adjusting the grip force further can influence the pressure difference between the control methods. The grip force is influenced by adjustments in the step size (React To Slip) and desired safety margin (Safety Margin Control). The following section illustrates the impact of altering the two control parameters.

	Mean (Pa)	Std (Pa)
Safety Margin Control	437	135
Conservative control	789	159
React To Slip	501	104

TABLE 2. Mean and standard deviation of maximum pressure per controller for all 27 objects.

6.3 Control parameters

Adjusting the desired safety margin (Γ_{des}) during Safety Margin Control, and the step size (F_{step}) during React to Slip, influences the observed maximum pressure and total lateral displacement (Fig. 17). The desired safety margin ranges from 9% to 80%, and the step size from 0.25 to 3 N.

First, it can be seen that a decrease in the desired safety margin results in a decrease in maximum pressure. The relative change in pressure scales with the relative change in safety margin. Furthermore, displacement is only observed for a desired safety margin of 9% and 10% due to overshoot of the controller. The overshoot is 10% and consequently the safety margin approaches 0% when the desired safety margin is lower than 10%. A 0% safety margin indicates slip which results in displacement. Safety Margin Control shows higher displacement and pressure than React To Slip when the desired safety margin is 9%.

Adjusting the step size has a similar effect. A decrease in step size results in a decrease in maximum pressure. The observed pressure scales with the step size. For a step size smaller than 0.5 N an increase in total displacement is observed.

7 Discussion

In this study, it is aimed to improve robotic grasping of fragile objects like fruit by developing a new

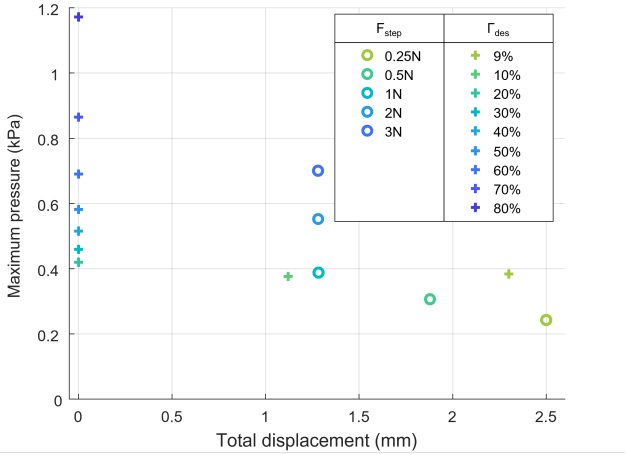

Fig. 17. Influence of adjusting the desired safety margin (Γ_{des}) during Safety Margin Control, and the step size (F_{step}) during React To Slip, on maximum pressure and total lateral displacement. The object's properties are: μ = 0.5, k_c = 200 kPa, and ρ = 0mm.

controller that uses tactile feedback to control the grip force. A model of a tactile sensor is created and the novel feedback controller (Safety Margin Control) is tested in simulation. Safety Margin Control estimates the safety margin and regulates the grip force to maintain a constant safety margin to hold various virtual objects in a stable grasp. Safety Margin Control is compared to two baseline controllers (React To Slip and Conservative Control). A robotic gripper should exert enough grip force to prevent slipping while being gentle enough to prevent damage to an object. Therefore, the performance is evaluated for maximum pressure and total lateral displacement between the object and sensor. Use of Safety Margin Control is expected to decrease fruit damage as the experiments resulted in a lower maximum pressure than the level that would lead to damage of a strawberry. Also, no slip occurred indicating that no fruits were falling to the ground. Conservative Control resulted in on average 44% higher pressure than Safety Margin Control, leading to damage to the fruit. React To Slip resulted in a constant displacement of 1.3 mm for each object, which is insufficient to release fruit from the gripper. Although it is difficult to regain a stable grasp after slip has occurred.

It is important to note that the observed displacement exactly approaches the threshold used to classify displacement as slip. The threshold might be unduly optimistic since a relative displacement of 15 mm between the object and the sensor was observed in the publication from which the threshold is obtained [18]. A displacement of 15 mm would probably result in object release considering the dimensions of a strawberry [31]. The difference between the used threshold of 1.3 mm and the relative displacement

of 15 mm originates from the following. In [18], an optical tactile sensor provided a distributed displacement field. The lowest observed displacement of a single node was 1.3 mm during the transition from stick to slip, hence the threshold was set to this value. However, the displacement was not measured relative to the object, but to the node's initial position. The threshold can be adapted in the simulation to obtain more realistic results. A threshold of 15 mm might be an exaggeration, since only a relative displacement of 2.6 mm between an object and sensor is shown to be sufficient for slip detection [19].

Trade-off between pressure and displacement

The relation between pressure and displacement is an inherent trade-off for manipulating fragile objects. Varying the desired safety margin offers a flexible way to tune the trade-off. For instance, by choosing a higher desired safety margin, no release is preferred over damage. Humans apply this strategy too. When a load is highly variable a higher safety margin is applied. Similar decision-making processes might be programmed into robotic grippers to enable dynamic controller adaptation based on the surroundings and external events. Safety Margin Control lends itself better to tune the trade-off than React To Slip, since it is not possible to completely eliminate displacement using React To Slip. Despite the inherent displacement, the lowest maximum pressure was observed during React To Slip for a small step size of 0.25 and 0.5 N. It can be said that React To Slip resembles 0-10% Safety Margin Control, as both methods show displacement and low pressure for these values. Safety Margin Control could be modified in order to maintain a desired safety margin of less than 10% without displacement, whereas it is not possible to completely eliminate displacement for React To Slip. The displacement in Safety Margin Control is caused by the controller's overshoot. Therefore, the proportional and integral gain were tuned, but the overshoot could not completely be removed. Future directions to consider are applying a ramping load rather than a step response, addition of a derivative term to the PI-controller, or using a different type of controller.

Friction coefficient estimation

Another important aspect of Safety Margin Control is its dependence on the object's friction coefficient. On initial contact, it is shown that the estimated friction coefficient (μ_{est}) only approached the real friction coefficient (μ_{real}) when μ_{real} = 0.3. To explain this observation it should be noted that μ_{est} only approaches μ_{real} when local slip occurs. The only force that can cause slip during initial contact is the elastic force of the sensor's membrane. This force only exceeded the threshold to slip when μ_{real} was 0.3, since the threshold to slip increases for an increasing real friction coefficient. The estimates for a real friction coefficient of 0.5 and 0.7 both approached 0.4 on initial contact. The estimates both approached their real value after a small load force was applied to the object causing local slip to occur. In this study, a load force was always present when Safety Margin Control was switched on. Therefore μ_{est} always approached μ_{real} and no problems related to the friction coefficient estimation were encountered. Nevertheless, a correct estimate is more important for experiments with the real sensor, because the friction coefficient can be location dependent (e.g. due to moist or sand) or vary over time (e.g. due to weather conditions). It has already been shown that the ChromaTouch sensor can be used to estimate the friction coefficient on initial contact [17]. However, only real friction coefficients of 0.1 and 0.4 were considered. It would be interesting to study if accurate estimates can be obtained for higher friction coefficients, since the present study encountered a threshold of μ_{real} = 0.4 to accurately estimate the friction coefficient on initial contact.

Tactile sensor model improvement

The Fingertip Model developed in [24] is used to model a tactile sensor. It takes both friction and viscoelasticity into account which are difficult to model [25], [26]. However, it faces problems regarding computational speed, and reliance on the initial nodes' configuration. Furthermore, the stiffness and damping parameters are tuned to the characteristics of a human finger rather than a tactile sensor. Therefore, the aim of this thesis was to enhance the Fingertip Model. The newly constructed model is referred to as the Sensor Model. A detailed explanation on the Sensor Model and comparison with the Fingertip model can be found in Appendix B. The Sensor Model is 20 times faster than the Fingertip Model. Additionally, it is adjustable to various sensor shapes and marker distributions. The increase in computational speed has two reasons. To begin with, a modification to the differential equations eliminated the need to store solutions to preceding time steps. Second, a different method to calculate the spring stiffnesses is implemented. The new method avoided the need to construct the large spring stiffness matrix that was required in the Fingertip Model. Repopulating the stiffness matrix took 90% of the computational time in the Fingertip Model. Also, this adaptation made the Sensor Model more adjustable to various sensor shapes and marker distributions. Despite these improvements, the Sensor Model could not be used to test the grip force controllers, as the deformation did not accurately reflect experimental data. However, it is recommended to develop the Sensor Model further. It could be used in more complex and real-time experiments (e.g. multiple or different tactile sensors) due to the increased speed and its adaptability. The main difference between both models lies in the Poisson effect which is implemented in the Fingertip Model,

but not accounted for in the Sensor Model (Appendix B.3.1). A good start would be to validate the Poisson implementation and study if it can improve the Sensor Model's results. Lastly, tuning of the model parameters (two spring stiffnesses and the damping coefficient) deserves special attention. Tuning these parameters proved to be very time-consuming in developing both the Fingertip and Sensor Model. At the same time, small adjustments had significant impact on the results. Therefore, more information on the influence of each parameter, how to obtain them, and their mutual relationship is required. Especially when the model is used to simulate various tactile sensors.

Recommendations

A model of a tactile sensor is used since it avoids the need for labor-intensive real-life tests and data augmentation. More realistic experiments (e.g. consider multiple sensors or rotation) can first be studied in simulation, before translating the current study to real-life which is the most important step for future work.

Rotation is very likely to occur when an object is held in a pinch grip, especially if the initial grip is not in line with the object's center of gravity. Motion that starts as a relative small rotation, can lead to an increased distance between the gripper and the object's center of gravity. Following this, the rotational speed could increase and result in object release from the gripper. Thus, rotation should be avoided to maintain a stable grasp. It would be interesting to add rotational slip to Safety Margin Control instead of considering translational slip alone. Other research already proved that it is possible to estimate the safety margin related to rotational slip, but did not implement it in a controller [16]. Also the friction coefficient was assumed to be constant and known in advance. It was shown that the safety margin had to be kept above a value of 50% in order to avoid rotational slip. This value is higher than the 10-40% that humans use for grip force control [8], suggesting that adding rotational slip might lead to the application of excessive grip force. It would be valuable to determine if rotation can be prevented for a lower safety margin.

When considering a multi-fingered robot hand it might not be desired to completely avoid both rotational and translational slip. Not all fingers are needed to maintain an object in a stable grasp, therefore finger placement can be controlled to execute dexterous manipulation tasks. The direction and magnitude of slip can provide useful information on finger placement relative to the object's center of gravity. The information from Safety Margin Control, i.e. how far a robotic fingertip is from slipping, could be used in planning algorithms used to determine where each finger should move next to execute the desired task. The first step to making this dexterous manipulation possible is to extend Safety Margin Control to multiple sensors and control the grip force of each sensor separately.

8 Conclusion

In this thesis a new way to control grip force is developed. Safety Margin Control is the first feedback controller that maintains a constant frictional safety margin based on tactile features. The performance of Safety Margin Control is evaluated in simulation against two baselines: Conservative Control and React To Slip. Safety Margin Control outperforms both baselines as it takes the importance of both object release and damage into consideration. The observed pressure is on average 44% lower than for Conservative Control. Also, no slip occurs, as opposed to React To Slip which results in 1.3 mm lateral displacement of the virtual objects relative to the sensor. The ability to adjust the desired safety margin provides a way to tune the trade-off between damage and release.

Safety Margin Control is a robust controller and can handle various object properties. It can be used to dynamically adapt the grip force taking changes in the environment or events that occur during grasping into consideration. Safety Margin Control can improve automated harvesting where robots have to manipulate fragile objects that vary in shape and size.

Acknowledgments

I would like to thank my supervisors Laurence Willemet, Michiel Plooij and Michaël Wiertlewski, for their guidance and support during my thesis project. Your enthusiasm kindled me to dive deeper into the topic and made me leave every meeting with increasing motivation.

References

[1] FAO, "World food and agriculture - statistical yearbook 2020." 2020, accessed: 2022-11-04. [Online]. Available: https://doi.org/10.4060/cb1329en

[2] Canadian Federation of Agriculture, "Getting into the field: Labour issues in agriculture," 2022, accessed: 2022-11-04. [Online]. Available: https://www.cfa-fca.ca/getting-into-the-field-labour-issues-in-agriculture/

[3] LTO Nederland, "Personeelstekort brengt oogstseizoen in gevaar," 2022, accessed: 2022-11-04. [Online]. Available: https://www.lto.nl/personeelstekort-brengt-oogstseizoen-in-gevaar/

[4] Environment, Food and Rural Affairs Committee (House of Commons), "Labour shortages in the food and farming sector," 2022, accessed: 2022-11-04. [Online]. Available: https://committees.parliament.uk/publications/9580/documents/162177/default/

[5] B. Zhang, Y. Xie, J. Zhou, K. Wang, and Z. Zhang, "State-of-the-art robotic grippers, grasping and control strategies, as well as their applications in agricultural robots: A review," Computers and Electronics in Agriculture, vol. 177, p. 105694, 2020.

[6] A. S. Augurelle, A. M. Smith, T. Lejeune, and J. L. Thonnard, "Importance of cutaneous feedback in maintaining a secure grip during manipulation of hand-held objects," Journal of neurophysiology, vol. 89, no. 2, pp. 665–671, 2003.

[7] G. Cadoret and A. M. Smith, "Friction, not texture, dictates grip forces used during object manipulation," Journal of neurophysiology, vol. 75, no. 5, pp. 1963–1969, 1996.

[8] A. M. Hadjiosif and M. A. Smith, "Flexible control of safety margins for action based on environmental variability," Journal of Neuroscience, vol. 35, no. 24, pp. 9106–9121, 2015.

[9] M. Al-Dairi, P. B. Pathare, R. Al-Yahyai, and U. L. Opara, "Mechanical damage of fresh produce in postharvest transportation: Current status and future prospects," Trends in Food Science & Technology, 2022.

[10] R. S. Johansson and A. B. Vallbo, "Tactile sensibility in the human hand: relative and absolute densities of four types of mechanoreceptive units in glabrous skin." The Journal of physiology, vol. 286, no. 1, pp. 283–300, 1979.

[11] F. Roël, "A Better Grasp on the Asymetrical Adaptation of Grip Force in Response to Friction Perturbations," Master's thesis, Delft University of Technology, Delft, July 2022.

[12] X. Lin and M. Wiertlewski, "Sensing the frictional state of a robotic skin via subtractive color mixing," IEEE Robotics and Automation Letters, vol. 4, no. 3, pp. 2386–2392, 2019.

[13] H. Sun, K. J. Kuchenbecker, and G. Martius, "A soft thumb-sized vision-based sensor with accurate all-round force perception," Nature Machine Intelligence, vol. 4, no. 2, pp. 135–145, 2022.

[14] Tactile Machines Lab, "Demo fuse gripper v1," 2022, Delft University of Technology.

[15] R. B. Scharff, D. J. Boonstra, L. Willemet, X. Lin, and M. Wiertlewski, "Rapid manufacturing of color-based hemispherical soft tactile fingertips," in 2022 IEEE 5th International Conference on Soft Robotics (RoboSoft). IEEE, 2022, pp. 896–902.

[16] P. Griffa, C. Sferrazza, and R. D'Andrea, "Leveraging distributed contact force measurements for slip detection: a physics-based approach enabled by a data-driven tactile sensor," in 2022 International Conference on Robotics and Automation (ICRA). IEEE, 2022, pp. 4826–4832.

[17] X. Lin, "Robotic touch for contact perception: Contributions to sensor design, manufacturing and signal processing," Ph.D. dissertation, Aix-Marseille Université, Marseille, 2020.

[18] J. W. James, N. Pestell, and N. F. Lepora, "Slip detection with a biomimetic tactile sensor," IEEE Robotics and Automation Letters, vol. 3, no. 4, pp. 3340–3346, 2018.

[19] S. Dong, W. Yuan, and E. H. Adelson, "Improved gelsight tactile sensor for measuring geometry and slip," in 2017 IEEE/RSJ International Conference on Intelligent Robots and Systems (IROS). IEEE, 2017, pp. 137–144.

[20] B. Ward-Cherrier, N. Pestell, L. Cramphorn, B. Winstone, M. E. Giannaccini, J. Rossiter, and N. F. Lepora, "The tactip family: Soft optical tactile sensors with 3d-printed biomimetic morphologies," Soft robotics, vol. 5, no. 2, pp. 216–227, 2018.

[21] S. Dong, D. Ma, E. Donlon, and A. Rodriguez, "Maintaining grasps within slipping bounds by monitoring incipient slip," in 2019 International Conference on Robotics and Automation (ICRA). IEEE, 2019, pp. 3818–3824.

[22] F. Veiga, B. Edin, and J. Peters, "Grip stabilization through independent finger tactile feedback control," Sensors, vol. 20, no. 6, p. 1748, 2020.

[23] J. W. James and N. F. Lepora, "Slip detection for grasp stabilization with a multifingered tactile robot hand," IEEE Transactions on Robotics, vol. 37, no. 2, pp. 506–519, 2020.

[24] L. Willemet, "On the biomechanics of the tactile perception of friction," Ph.D. dissertation, Aix-Marseille Université, Marseille, 2021.

[25] F. F. Abayazid and M. Ghajari, "Material characterisation of additively manufactured elastomers at different strain rates and build orientations," Additive Manufacturing, vol. 33, p. 101160, 2020.

[26] M. Urbakh, J. Klafter, D. Gourdon, and J. Israelachvili, "The nonlinear nature of friction," Nature, vol. 430, no. 6999, pp. 525–528, 2004.

[27] P. R. Dahl, "Solid friction damping of mechanical vibrations," AIAA journal, vol. 14, no. 12, pp. 1675–1682, 1976.

[28] M. Otsuki and H. Matsukawa, "Systematic breakdown of amontons' law of friction for an elastic object locally obeying amontons' law," Scientific reports, vol. 3, no. 1, pp. 1–6, 2013.

[29] F. Veiga, H. Van Hoof, J. Peters, and T. Hermans, "Stabilizing novel objects by learning to predict tactile slip," in 2015 IEEE/RSJ International Conference on Intelligent Robots and Systems (IROS). IEEE, 2015, pp. 5065–5072.

[30] M. M. Özcan and H. Hacıseferoğulları, "The strawberry (arbutus unedo l.) fruits: chemical composition, physical properties and mineral contents," Journal of Food Engineering, vol. 78, no. 3, pp. 1022–1028, 2007.

[31] L. M. Oo and N. Z. Aung, "A simple and efficient method for automatic strawberry shape and size estimation and classification," Biosystems engineering, vol. 170, pp. 96–107, 2018.

[32] X. An, Z. Li, M. Zude-Sasse, F. Tchuenbou-Magaia, and Y. Yang, "Characterization of textural failure mechanics of strawberry fruit," Journal of Food Engineering, vol. 282, p. 110016, 2020.

[33] K. Johnson, "Tangential loading and sliding contact," in Contact Mechanics. Cambridge University, 1985, ch. 7, pp. 202–241.

APPENDIX A
NOMENCLATURE

Symbol	Definition	Unit
c	damping coefficient	Ns/m
F_f	friction force	N
F_{grip}	grip force	N
F_n	normal contact force	N
F_{spring}	spring force	N
k	spring stiffness	N/m
l	spring length	m
n	material parameter	-
N_n	number of nodes	-
r	radius	m
s	state	-
x, y	position	m
$\Delta x, \Delta y$	displacement	m
$\dot{x}, \dot{y}$	velocity	m/s
α	angle	rad
Γ	safety margin	%
ρ	curvature	m
μ	friction coefficient	-
σ_0	stiffness of the bristle (Dahl model)	N/m
ν	Poisson factor	-

APPENDIX B
SENSOR MODEL

A model of a tactile sensor is created to test the performance of Safety Margin Control in simulation. The tactile sensor is modeled using the numerical two-dimensional model of a fingertip developed in [24], called the Fingertip Model. The Fingertip Model takes both friction and viscosity into account, which are difficult to model [25], [26]. At the same time, it only needs 4 parameters (2 spring stiffnesses, damping coefficient and finger radius) to predict mechanical deformation and contact forces during interaction with objects of varying properties (curvature, stiffness and friction coefficient). However, it faces problems regarding computational speed, and reliance on the initial nodes' configuration. Also, the stiffness and damping parameters are fitted to the characteristics of a human finger instead of a tactile sensor. Therefore, the aim of this study was to enhance the existing Fingertip Model. The newly constructed model is referred to as the Sensor Model. The basic model structure is kept the same and Fig. 18 shows the complete model. The nomenclature can be found in Appendix A.

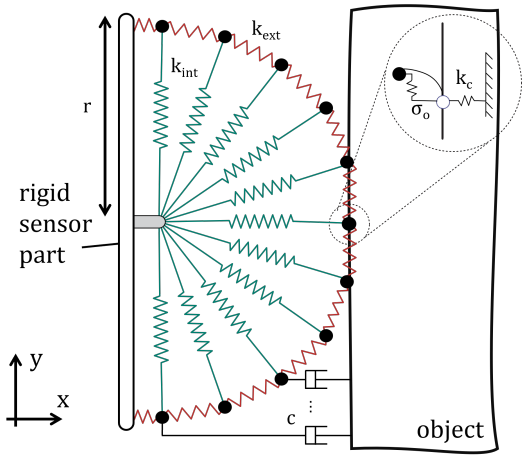

Fig. 18. Basic model structure where nodes (black) are connected via springs and dampers. Model parameters k_{int} and k_{ext} represent the stiffnesses of the internal (green) and external (red) springs, respectively. c is the damping coefficient and r the sensor radius. The parameters k_c and σ_0 define the contact between the sensor and the object.

In this appendix, the Fingertip and Sensor Model are compared. The conclusion is provided here and the subsequent sections contain more detailed information. The Sensor Model is 20 times faster than the Fingertip Model, because of two reasons. Firstly, an adaptation to the differential equations avoided the need to store solutions to preceding time steps (section B.2). Secondly, the computational speed improved by implementing a more general way to calculate the spring forces (section B.3). Additionally, this adaptation made the Sensor Model more adjustable to various sensor shapes or marker distributions than the Fingertip Model (section B.3). The Fingertip Model outperformed the Sensor Model when comparing the models' output to real sensor data. The difference lies in the spring force calculation with special attention for the implementation of the Poisson effect (section B.3.1). It is tried to improve the performance of the Sensor Model by adjusting the spring stiffnesses, but no values that provided realistic results both during initial contact and sliding were obtained (section B.3.2).

Despite the improvements, the Sensor Model could not be used to test the grip force controllers, as the deformation did not accurately reflect experimental data. However, it is recommended to develop the Sensor Model further. It could be used in more complex and real-time experiments (e.g. multiple or different tactile sensors) due to the increased speed and its adaptability. The main difference between both models lies in the Poisson effect which is implemented in the Fingertip Model, but not accounted for in the Sensor Model. A good start would be to validate the Poisson implementation and study if it can improve the Sensor Model's results.

B.1 Dynamics

The Sensor Model employs the same equations of motion as the Fingertip Model (section 3). Only the spring stiffnesses are maintained constant, therefore the internal and external spring stiffnesses are represented by a constant rather than a stiffness matrix (12).

$$c \begin{bmatrix} \vec{\dot{x}} \\ \vec{\dot{y}} \end{bmatrix} + k \begin{bmatrix} \vec{\Delta x} \\ \vec{\Delta y} \end{bmatrix} + \begin{bmatrix} \vec{F}_x \\ \vec{F}_y \end{bmatrix}_{ext} = 0 \tag{12}$$

B.2 Contact interaction

The contact forces are calculated using the same approach as the Fingertip Model (section 3). The only difference is the way the friction force is accounted for in the differential equation. The Fingertip Model's

state vector is defined by $\vec{s} = [\vec{x},\ \vec{y}]$, where $\vec{x}$ and $\vec{y}$ represent the displacement of each node. Whereas in the Sensor Model, the friction force (F_f) is added to the state. Therefore, the state vector becomes $\vec{s} = [\vec{x},\ \vec{y},\ \vec{F}_f]$. The reason for this adaptation is that the lateral speed is required to calculate the friction force using the Dahl model [27]. The Fingertip Model stored solutions to preceding time steps to obtain the lateral speed, but this loop is avoided by adding the friction force to the state vector (13). The third differential equation represents the Dahl equation. For clarity, the lateral speed is written as $\dot{y}$ in the Dahl equation, but it is actually replaced by the solution to the second differential equation.

$$\begin{bmatrix} \dot{\vec{x}} \\ \dot{\vec{y}} \\ \dot{\vec{F}}_f \end{bmatrix} = \begin{bmatrix} -c^{-1} \cdot \vec{F}_{ext,x} - c^{-1} \cdot k \cdot \vec{x} \\ -c^{-1} \cdot \vec{F}_{ext,y} - c^{-1} \cdot k \cdot \vec{y} \\ \sigma_0 \cdot \left| 1 - \frac{F_f}{\mu \cdot F_n} \operatorname{sign}(\dot{y}) \right|^n \cdot \operatorname{sign}\left(1 - \frac{F_f}{\mu \cdot F_n} \operatorname{sign}(\dot{y})\right) \cdot \dot{y} \end{bmatrix} \tag{13}$$

B.3 Spring forces

The primary distinction between the Sensor and Fingertip Model is the way the spring forces are calculated. The Fingertip Model divides a spring connecting two nodes into a horizontal and a vertical component (Fig. 19a). The Sensor Model considers a single spring that connects two nodes (Fig. 19b).

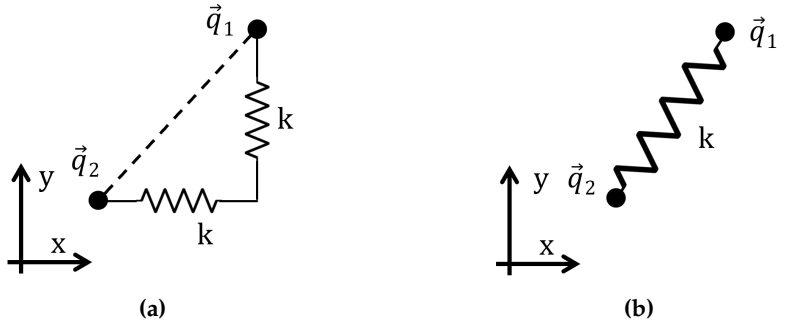

Fig. 19. Definition of a spring connecting two nodes (a) Fingertip Model. (b) Sensor Model.

The Sensor Model applies Hooke's law ($F = -k \cdot \Delta l$) to calculate the force induced by a spring. The obtained force acts in line with the spring and can be split in a horizontal and vertical component (14). Here, Δl represents the length change of the spring, vector $\vec{q_i}$ defines the position of a node ($\vec{q_i} = [x_i,\ y_i]$), and k is the spring stiffness. The Fingertip Model uses a different equation, where the spring stiffness is split in a horizontal and a vertical component (15). Here, $k_x = k \cdot \cos\alpha$ and $k_y = k \cdot \sin\alpha$.

$$\vec{F}_{spring} = \begin{bmatrix} \mathrm{F}_{\mathrm{spring,x}} \\ \mathrm{F}_{\mathrm{spring,y}} \end{bmatrix} = -k \cdot \Delta l \cdot \frac{(\vec{q}_1 - \vec{q}_2)}{|\vec{q}_1 - \vec{q}_2|} \tag{14}$$

$$\begin{aligned} F_{spring,x} &= k_x \cdot \Delta x - k_y \cdot \nu \cdot \Delta y \\ F_{spring,y} &= k_y \cdot \Delta y + k_x \cdot \nu \cdot \Delta x \end{aligned} \tag{15}$$

The two implementations are compared in more detail by considering a single spring. Two simple configurations are studied. In either example an initially unstretched spring is compressed by an external force. Following this, the spring will deform and the nodes will displace accordingly. Both models are used to simulate the motion until a steady state is reached. The first example is a vertical spring (Fig. 20a). The surface prevents the bottom node from moving down and only the upper node displaces in vertical direction. Indeed no motion in horizontal direction (x) is expected, since the force is applied in line with the spring. However, the spring rotates in the Fingertip Model (Fig. 20b).

A spring is positioned under an angle of 45 degrees with the frictionless surface in the second example (Fig. 21a). The downward force pushes the upper node down and the bottom element can move freely over the surface. The spring force acts in line with the spring in the Sensor Model and therefore nothing opposes the external force. Consequently, a steady state is reached when the spring lies in a horizontal position on the surface (orange line in Fig. 21b). By contrast, in the Fingertip Model, the vertical component of the spring directly opposes the applied force. In this case, a different steady state is observed (blue line in Fig. 21b).

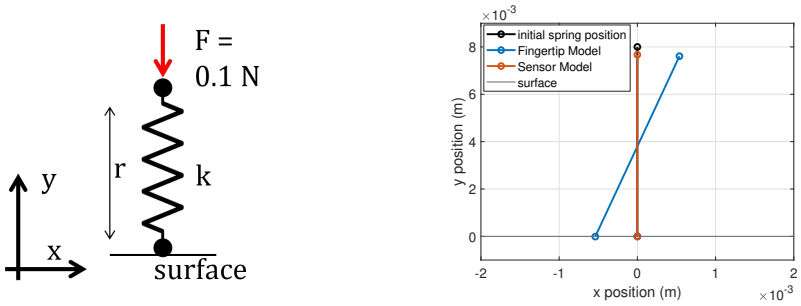

(a) (b)

Fig. 20. (a) Vertical spring under compression. The surface is frictionless and the nodes can move freely over it. k = 314 N/m, r = 8 mm and damping factor c = 0.1 Ns/m. The Poisson effect in the Fingertip Model is 0.4. (b) Simulated steady state when external force is applied.

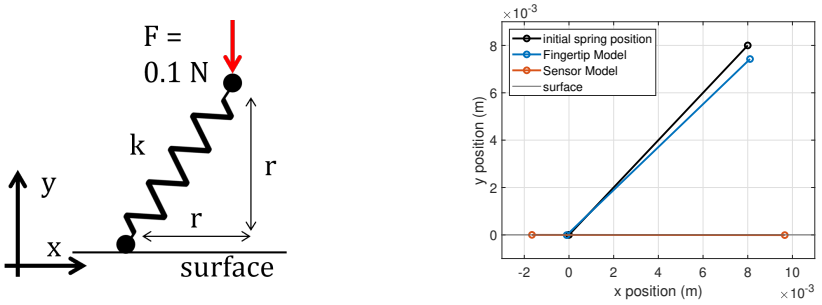

(a) (b)

Fig. 21. (a) Rotated spring under compression. The surface is frictionless and the nodes can move freely over it. k = 314 N/m, r = 8 mm and damping factor c = 0.1 Ns/m. The Poisson effect in the Fingertip Model is 0.4. (b) Simulated steady state when external force is applied.

Both spring force implementations for a single spring are extended to the complete model with multiple springs. The internal and external springs have different stiffnesses, respectively k_{int} and k_{ext}. However, the stiffnesses in the Fingertip Model depend on the orientation of the springs, so setting an initial stiffness does not mean that the stiffness constantly maintains this value during the simulation. Nevertheless, both models are compared for the same initial stiffnesses and the simulated results are presented here. Instead of a single spring, the complete model is now pressed against a frictionless surface due to an externally applied load (Fig. 22a). The simulated results are presented for the resulting steady state.

First, the normal contact force acting on the nodes in contact with the surface is displayed. Both models obtain a similar normal contact force (Fig. 22b). The x component of the internal springs almost exactly opposes the normal contact force (Fig. 22d), because no other forces act on the nodes. The x component of the external springs only has a small effect, since these springs are oriented tangentially to the surface (Fig. 22f). However, the y component of both the internal and external springs shows more contrast (Fig. 22c and 22e). The external spring force exactly opposes the internal spring fore, due to the fact that the surface is frictionless and no other vertical forces are present. Considering the internal springs, the x component is five times lower in the Sensor Model than in the Fingertip Model. Also, the distribution is different. The vertical force in the Fingertip Model mainly relies on the Poisson effect, which causes an expansion of the model perpendicular to the applied load. The implementation of the Poisson effect is studied in more detail, since the Sensor Model did not implement it in the spring force calculation.

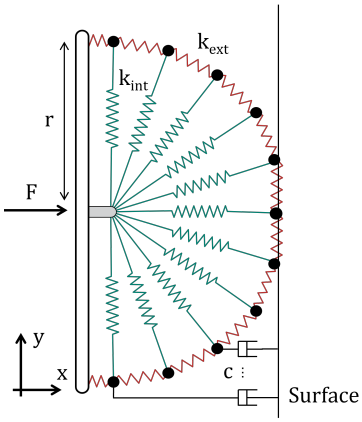

(a) F = 1 N, k_{int} = 314 N/m, k_{ext} = 1544 N/m, c = 0.1 Ns/m, and r = 8 mm.

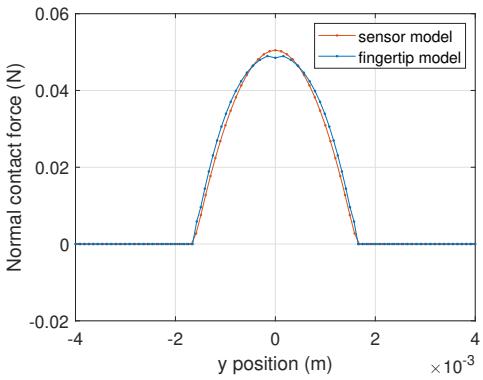

(b) Normal contact force sensor and Fingertip Model.

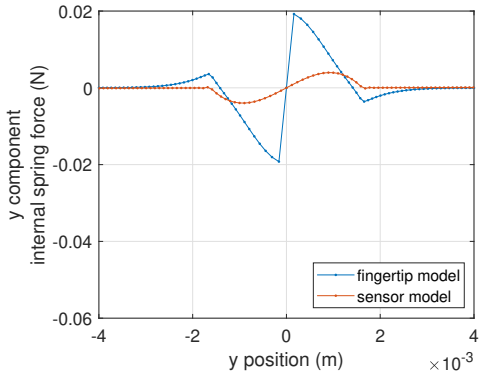

(c) y component internal springs.

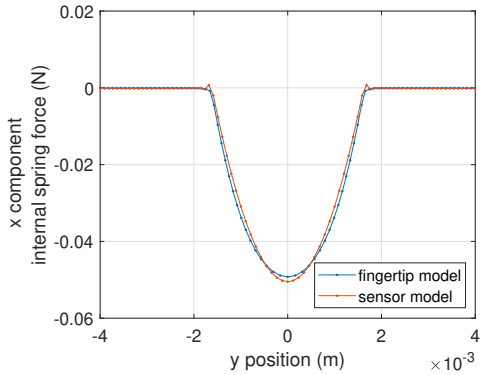

(d) x component internal springs.

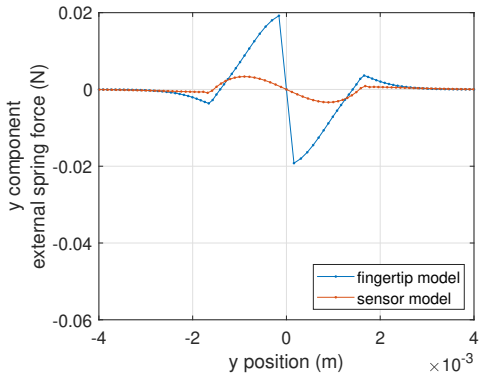

(e) y component external springs.

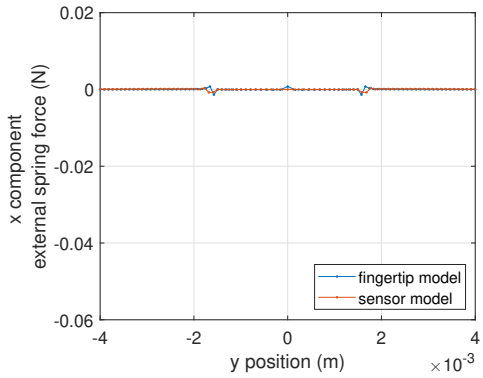

(f) x component external springs.

Fig. 22. Spring forces of nodes in contact with the surface for both the Fingertip and Sensor Model. The sensor is pressed against a frictionless surface. The spring forces are presented when a steady state is reached. The Poisson effect is added in the Fingertip Model and ν_{int} = 0.4 (internal springs) and $\nu_{ext} = 0.004$ (external springs).

B.3.1 Poisson effect

In Fig. 22d it was observed that the x component of the internal springs followed a parabolic distribution for the nodes in contact with the surface. The largest absolute horizontal force acts on the central node and its magnitude is 0.05 N. With this in mind, it is important to note that the internal springs in contact with the surface are approximately oriented horizontally. So, the y component of the spring force is equal to the Poisson factor times the x component (= 0.4 $\cdot F_{spring,x}$). And indeed, the y component of the internal spring force shows a peak at 0.02 N (Fig. 22c). The Poisson effect is not considered for the central node, therefore the magnitude equals zero at a y position of 0 m. The direction of the vertical force is hard coded and depends on the position of a node relative to the central node. As a consequence, the vertical spring force is negative for a negative y position and positive for a positive y position.

Interestingly, the Poisson effect is implemented counter intuitively. Poisson's law states that $\nu = -\frac{\Delta y}{\Delta y'}$ for a material under compression, therefore $\Delta y' = -\nu \cdot \Delta y$ (Fig. 23a). The horizontal spring force is then calculated according to equation 16 in the Fingertip Model (Fig. 23b). In this example Δx equals zero, since only a vertical force is applied and initially no horizontal displacement occurs.

$$F_{spring,x} = k_x \cdot \Delta x - k_y \cdot \Delta y' \tag{16}$$

Since $\Delta y'$ is a horizontal displacement it should be multiplied with the horizontal spring stiffness (17). This implementation of the Poisson effect will be referred to as the inverse Poisson implementation.

$$F_{spring,x} = k_x \cdot \Delta x - k_x \cdot \Delta y' \tag{17}$$

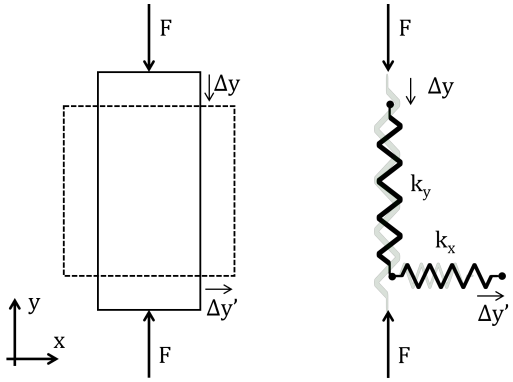

(a) Poisson effect general. **(b)** Poisson effect springs.

Fig. 23. Schematic of the Poisson effect.

The lateral displacement is used in order to study the effect of the inverse Poisson implementation. Experimental data of a tactile sensor with a radius of 10 mm was available. The sensor was pressed against a surface with a friction coefficient of 0.1. The Fingertip and Sensor Model are set to the same values (Fig. 24a). The lateral displacement of the Fingertip Model better matched the experimental data than the Sensor Model based on the magnitude of the displacement. Although, the Sensor Model's marker position of the peak displacement overlapped better with the experimental data. The Fingertip Model with inverse Poisson implementation shows a different result than the normal Fingertip Model (Fig. 24b). It is plotted in a separate graph to display the shape of the graph better. The magnitude of the lateral displacement decreases compared to the Fingertip Model and the peak shifts outward. The shape of the Fingertip Model with inverse Poisson implementation resembles the shape of the Sensor Model more than the normal Fingertip Model. Due to time constraints, it is not tried to tune the Poisson ratio and spring stiffnesses further to validate if the inverse Poisson implementation can provide more realistic results.

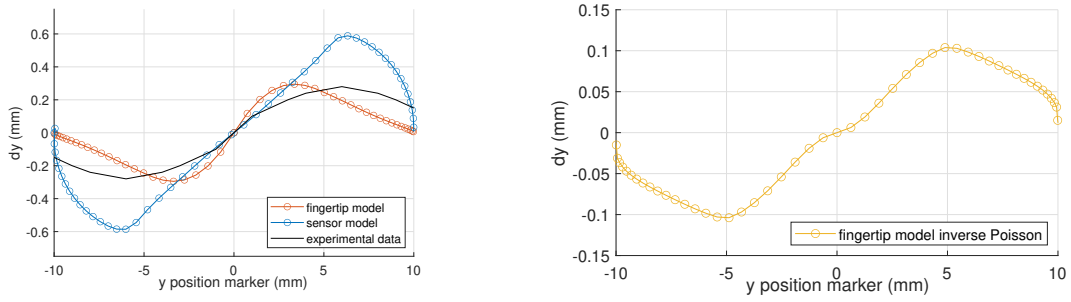

(a) **(b)**

Fig. 24. Lateral displacement. The radius of the sensor is 10 mm. (a) Fingertip Model, Sensor Model, and experimental data. (b) Fingertip Model with inverse Poisson implementation.

B.3.2 Adjustments to initial spring stiffnesses

Furthermore, the influence of adjusting the internal and external springs stiffnesses is studied. The effect of adjusting the spring stiffnesses is shown by means of the following example. The sensor is pressed against a surface and afterwards an orthogonal load is applied (Fig. 25). This time friction is considered, but the load is smaller than μF_n, so no sliding should occur. The simulated result are shown when a steady state is reached (Fig. 26a). The Fingertip Model indeed reaches a stable situation without relative lateral motion between the sensor and contact. However, the Sensor Model shows different results. The external layer of springs stretches and lateral motion occurs before the simulation reaches a steady state. In order to reduce the stretching, the external spring stiffness is increased with a factor 20. In this case, no stretching occurs and the sensor shows less lateral motion (Fig. 26b). This observation is more realistic, but increasing the external spring stiffness also has an undesired effect.

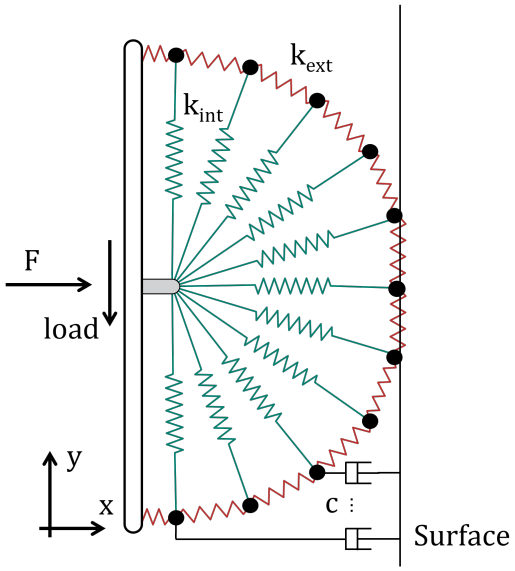

Fig. 25. Load $< \mu F_n$, so no sliding should occur.

To illustrate the undesired effect of increasing the external spring stiffness another simulation is studied. Now the sensor is pressed on a surface, but no load is applied. Friction is considered and μ = 0.5. The contact forces are shown for a steady-state (Fig. 27). In the Sensor Model, the force vectors point outward for the nodes at the edges of the contact (Fig. 27a). Whereas in the Fingertip Model all vectors point inward (Fig. 27b). According to literature inward pointing force vectors are expected [33].

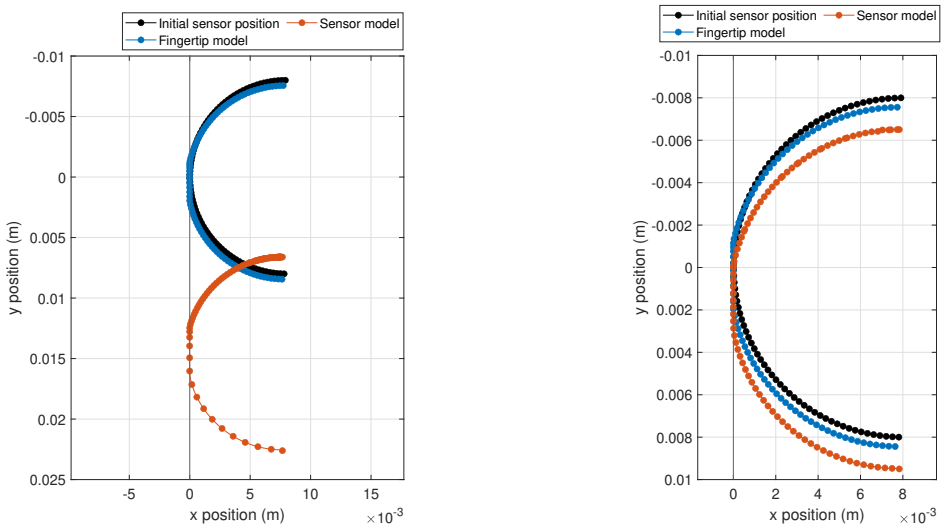

Fig. 26. Simulated results for μ=0.5, k_{int}=314 N/m, and c = 0.1 Ns/m. k_{ext} is varied. (a) k_{ext}=1544 N/m (b) k_{ext}= 30 kN/m.

In summary, adjusting the spring stiffnesses resulted in some situations in more realistic simulations, but no general set of parameters was obtained that provided realistic results during both initial contact and sliding.

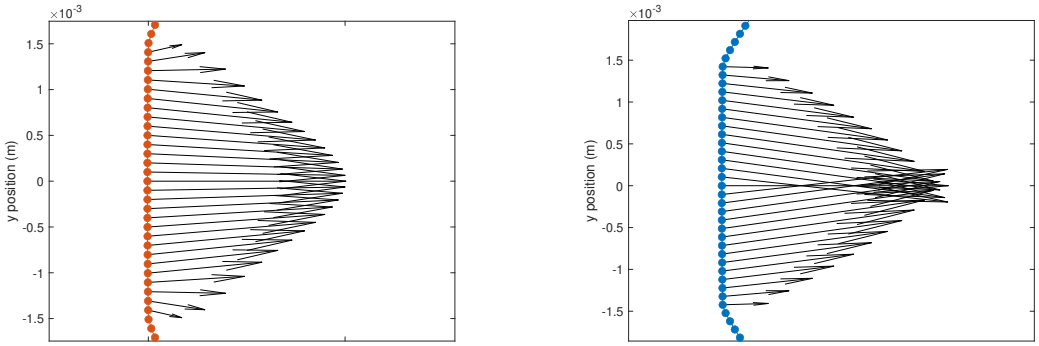

(a) Sensor Model. **(b)** Fingertip Model.

Fig. 27. Force vectors at contact when sensor is pressed against the surface. The external spring stiffness k_{ext} = 30 kN/m. The friction coefficient is 0.5. The vectors are shown when a steady-state is reached.